RESEARCH ARTICLE
ATMOSPHERIC PHYSICS

*Earth and Planetary Physics*
*3*: 126–135, 2019
doi: 10.26464/epp2019016

# Application of cloud multi-spectral radiances in revealing cloud physical structures

**Juan Huo*, DaRen Lu, and WenJing Xu**

Key Laboratory for Atmosphere and Global Environment Observation, Chinese Academy of Sciences, Beijing 100029, China

**Abstract:** The radiances scattered or emitted by clouds demonstrate diverse features at different wavelengths due to different cloud physical structures. This paper presents a method (the smallest-radiance-distance method, SRaDM) of revealing the physical structures of clouds. The method is based on multi-spectral radiances measured by the Moderate Resolution Imaging Spectroradiometer (MODIS) onboard Aqua. The principle and methodology of SRaDM is deduced and provided in this paper. Correlation analysis based on data from MODIS and Cloud Profiling Radar (onboard CloudSat), collected from January 2007 to December 2010 over an ocean area (15°N–45°N, 145°E–165°E), led to selection of radiances at 13 wavebands of MODIS that demonstrated high sensitivity to cloud physical structures; radiances at the selected wavebands were subjected to SRaDM. The Standardized Euclidean distance is introduced to quantify the degree of changes in multi-spectral radiances (termed $D_{rd}$) and in physical structures (termed $D_{st}$) between cloud profiles. Statistics based on numerous cloud profiles show that $D_{rd}$ decreases monotonically with a decrease in $D_{st}$, which implies that small $D_{rd}$ always accompanies small $D_{st}$. According to the law of $D_{rd}$ and $D_{st}$, the new method, SRaDM, for revealing physical structures of clouds from the collocation of cloud profiles of similar multi-spectral radiances, is presented. Then, two successful experiments are presented in which cloud physical structures are captured using multi-spectral radiances. SRaDM provides a way to obtain knowledge of the physical structures of clouds over relatively larger areas, and is a new approach to obtaining 3D cloud fields.

**Keywords:** cloud; physical structure; radiance; radar

**Citation:** Huo, J., Lu, D. R., and Xu, W. J. (2019). Application of cloud multi-spectral radiances in revealing cloud physical structures. *Earth Planet. Phys.*, *3*(2), 126–135. http://doi.org/10.26464/epp2019016

## 1. Introduction

Remote sensing of clouds has two modes: the passive mode and the active mode. In the passive mode, some physical parameters of clouds, such as particle size and cloud top height, have been retrieved from radiances measured at different spectral bands (Nakajima and King, 1990; Baum et al., 2012; Marchand, 2013). Multi-spectral radiances scattered or emitted by clouds are related to the physical properties of clouds. The passive mode dominates cloud remote sensing due to its advantages, such as ease of maintainability and lower economic cost relative to the active mode. A significant drawback of the passive mode, however, is its inability to explore the interior structures of clouds. In contrast, radar—a typical instrument of the active mode—shows powerful ability in exploring the structure of clouds (Sekelsky, 1999; Heymsfield et al., 2014; Görsdorf et al. 2015).

There are few observations available of cloud macro- and micro-physical properties in 3D because of limitations of detection technologies and lack of financial support. Currently, therefore, 3D cloud fields applied in 3D radiative transfer models are mostly generated by models—for example, large eddy simulation models or stochastic cloud generation models (Stevens et al., 1999; Khairoutdinov and Kogan 2000; Prigarin and Marshak 2009; Alexandrov et al., 2010). Such models use numerical approaches to simulate and generate 3D cloud fields.

Remote sensing in the passive mode on satellite platforms has collected far more cloud data than the active mode, and generally covers broader areas. Barker et al. (2011) presented an algorithm to generate the three-dimensional cloud field based on four spectral bands according to the EarthCARE detection mission. CloudSat and Aqua are members of the Afternoon Satellite Constellation (A-train, http://cloudsat.atmos.colostate.edu/publications, A-Train Fact Sheet). Aqua flies ahead of CloudSat by about 1.5 minutes. On the Aqua satellite, the Moderate Resolution Imaging Spectroradiometer (MODIS) performs radiative observations at 36 spectral wavebands (https://modis-atmos.gsfc.nasa.gov/). CloudSat, meanwhile, is equipped with a W-band (94-GHz) millimeter-wave cloud profiling radar (CPR, http://www.cloudsat.cira.colostate.edu/). CPR detects the vertical structures of clouds and precipitation on the flight path with a breadth of about 1.4 km. Comparatively, MODIS measures a much larger area (2330 km across-track) than CPR. In this paper, we attempt to reveal the physical structures of clouds around the CPR flight path based on multi-spectral radiances measured by MODIS, thus providing empirical knowledge of cloud physical structures over relatively larger areas. This work presents a new approach to obtaining 3D cloud fields, a method that we refer to as the 'smallest-radiance-

Correspondence to: J. Huo, huojuan@mail.iap.ac.cn
Received 31 JAN 2019; Accepted 14 MAR 2019.
Accepted article online 25 MAR 2019.

distance method', hereafter abbreviated to SRaDM. In this paper, the spectral bands of MODIS applicable in SRaDM are analyzed based on four years of data over an ocean area. To study the relationship between spectral radiance and physical structure, a Standardized Euclidean distance is introduced to quantify the difference in radiative and physical properties of cloud pixels.

Following this introduction, Section 2 describes the instruments (i.e., MODIS and CPR) and their products. In Section 3, the 36 wavebands of MODIS are analyzed to understand their interrelationships and their sensitivities to cloud physical structures. In Section 4, a detailed theoretical analysis and the approach to deriving cloud physical structures from multi-spectral radiances are provided. In Section 5, the results from experiments designed to reveal cloud physical structures are presented. The last section is a summary of the study's key findings.

## 2. Data

The footprint of MODIS is about 10 km (along-track) by 2330 km (across-track). MODIS measures radiance at 36 spectral bands ranging from 0.4 to 14.4 μm (Ackerman et al., 2008; Frey et al., 2008). There are 22 spectral bands that can be utilized to explore optical and physical properties (e.g., height, depth, water path) of clouds. These 22 wavebands cover the visible, near-infrared, and thermal infrared bands (see Table 1). The spatial resolution of radiance in wavebands 1 and 2 is 250 m, 500 m in wavebands 3–7, and 1 km in wavebands 8–36. Radiances at waveband 6 are unreliable because of noise problems.

The footprint of the CloudSat product is approximately 1.7 km (along-track) by 1.4 km (across-track), and the vertical resolution is 240 m. All standard cloud products, such as 1B-CPR (radar backscatter profiles), 2B-CWC-RVOD (combined water-content radar+visible optical depth), and 2C-ICE products (Winker et al., 2009), are produced at the CloudSat Data Processing Center (http://cloudsat.atmos.colostate.edu/data). A brief diagram illustrating the footprints of MODIS and CPR products is given in Figure 1. As shown in Figure 1, the footprint of MODIS completely covers that of CPR. Assuming that the lower-left pixel along the flight direction is number one, the eighth MODIS grid has the closest position among the 15 grids to the CPR profile. Radiances of the eighth grid are used as that of the CPR profile.

To match the spatial resolution of the CPR cloud profile, radiances of 1-km resolution are used in this study. All the data utilized in this paper were collected from January 2007 to December 2010 over an ocean area (15°N–45°N, 145°E–165°E).

## 3. Spectral Bands Used in SRaDM

The radiances obtained by MODIS include solar or thermal radi-

**Table 1.** The 22 wavebands of MODIS applied for cloud detection

| Waveband | Band width | Resolution | Primary usage |
|---|---|---|---|
| 1 | 620–670 nm | 250 m | Surface/Cloud/Aerosol boundary |
| 2 | 841–867 nm | 250 m | Surface/Cloud/Aerosol characteristics |
| 3 | 459–479 nm | 500 m | |
| 4 | 545–565 nm | 500 m | |
| 5 | 1230–1250 nm | 500 m | |
| 6 | 1628–1652 nm | 500 m | |
| 7 | 2105–2155 nm | 500 m | |
| 17 | 890–920 nm | 1000 m | Cloud/Atmosphere vapor |
| 18 | 931–941 nm | 1000 m | |
| 19 | 915–965 nm | 1000 m | |
| 20 | 3.66–3.84 μm | 1000 m | Surface/Cloud temperature |
| 26 | 1.36–1.39 μm | 1000 m | Cirrus/Vapor/Humidity |
| 27 | 6.535–6.895 μm | 1000 m | |
| 28 | 7.175–7.475 μm | 1000 m | |
| 29 | 8.4–8.7 μm | 1000 m | Cloud properties |
| 30 | 9.58–9.88 μm | 1000 m | Ozone/Cloud properties |
| 31 | 10.78–11.28 μm | 1000 m | Surface/Cloud temperature |
| 32 | 11.77–12.27 μm | 1000 m | Cloud height/Surface temperature |
| 33 | 13.185–13.485 μm | 1000 m | Cloud height/Cloud cover |
| 34 | 13.485–13.785 μm | 1000 m | |
| 35 | 13.785–14.085 μm | 1000 m | |
| 36 | 14.085–14.385 μm | 1000 m | |

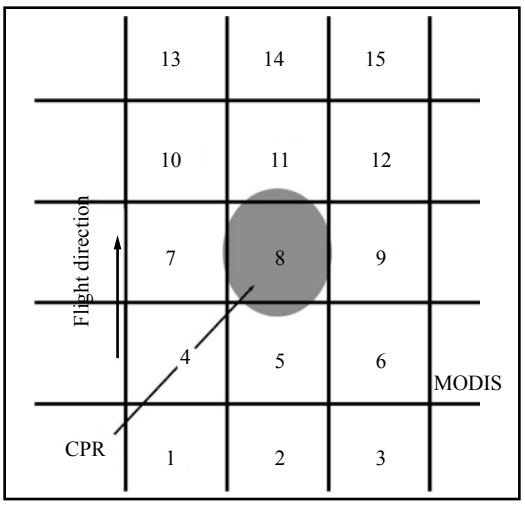


**Figure 1**. Illustration of the footprints of MODIS and CPR. Each box represents one MODIS grid. The gray ellipse represents the footprint of CPR.

ation reflected or emitted by clouds, the surface, the atmosphere, and so on. The 22 spectral bands (in Table 1) are designed to measure different cloud physical characteristics. For example, radiances at infrared bands are closely related to the cloud-top pressure; the combination of radiances at visible and near-infrared bands is applicable in estimating cloud optical thickness and cloud effective radius. Radiances at one single waveband might be highly sensitive to a particular physical property of clouds. Other cloud properties might be detected by combinations of radiance data from two or more spectral wavebands. Radiances at particular spectral bands might show weak sensitivity to a particular cloud physical property. Thus, although radiances at different spectral bands are known to have reflected cloud physical properties, the roles that they might play in revealing such physical details have been uncertain. It has thus been necessary to investigate which spectral bands and combinations of bands from the 22 available wavebands can best be used to represent various physical properties of clouds.

A case in Figure 2 shows the variation of radiances at different spectral bands when the cloud physical structure changes. Figure 2a shows the radar reflectivity factors ($Z_e$; units: dBZ) measured by CPR on 14 August 2007. Figure 2b displays the corresponding MODIS radiances (units: W/m$^2$·μm·sr) at 21 wavebands. To show all radiances with one color map, radiances at wavebands 20 and 29–36 are magnified by a factor of 10, and the radiances at wavebands 26–28 are magnified by a factor of 100. As shown in Figure 2, radiances at wavebands 1, 3, and 4 increase greatly for thick cloud profiles; the radiances at wavebands 29, 31, and 32 show an opposite distribution relative to that of wavebands 1, 3, and 4; and radiances at wavebands 29, 31, and 32 show similar variations. It is

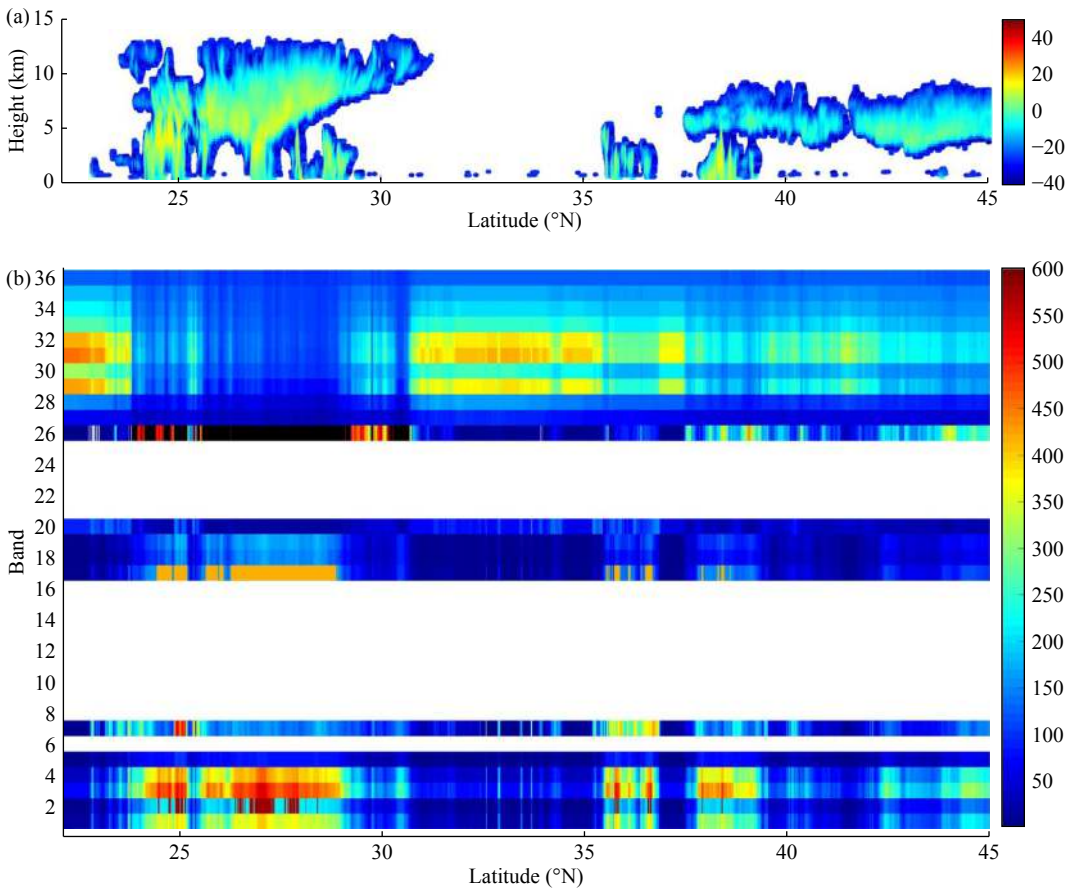


**Figure 2**. Clouds measured on 14 August 2007 over (15°N–45°N, 145°E–165°E) by CPR and MODIS: (a) radar reflectivity factors of cloud profiles collected by CPR; (b) radiances at 21 spectral bands measured by MODIS.

apparent that the radiances at each waveband change differently along with different cloud profiles.

To identify those wavebands that demonstrate similar variations, Pearson's correlation coefficient (hereinafter referred to as $P_{cc}$) is introduced. Pearson's correlation coefficient is the covariance of two variables divided by the product of their standard deviations. Given a pair of random variables ($A$, $B$), the formula for $P_{cc}$ is

$$P_{cc}(A,B) = \frac{\mathrm{cov}(A,B)}{\sigma_A \sigma_B}, \tag{1}$$

where 'cov' is the covariance, $\sigma_A$ is the standard deviation of $A$, and $\sigma_B$ is the standard deviation of $B$. The $P_{cc}$ values between the 22 wavebands for the clouds in Figure 2 are given in Figure 3. The color of each block represents the $P_{cc}$ between two wavebands, which are labeled by the abscissa and ordinate. As shown in Figure 3, the $P_{cc}$ values between bands 1, 3, and 4 are greater than 0.9, which means that radiances at wavebands 1, 3, and 4 change similarly to each other when the cloud physical structure changes. Here, one of the three wavebands can be picked out and used as a representative waveband.

All of the radiances of the clouds at the 22 wavebands collected from January 2007 to December 2010 are analyzed to find those wavebands that are highly correlated to cloud physical structures. The results are presented in Figure 4. It can be seen that the variations of some wavebands correspond closely with changes in cloud physical structures, which indicates that they are highly sensitive to cloud physical properties. From Figure 4, wavebands 1–4 and 17 show highly positive correlations to each other. Wavebands 18 and 19 also show high positive correlations. In addition, positive high correlations can be found among wavebands 29, 31, and 32, as well as between wavebands 34 and 35. Within each group of wavebands exhibiting close positive relationships to each other, one waveband can be chosen as a representative to convey the particular characteristic of cloud physical structure that the group detects. Choosing a single waveband for a particular characteristic also serves to balance the weights of the spectral bands in the expressions of radiative properties of clouds. According to the correlation analysis, it is found that wavebands 01, 05, 07, 18, 20, 26, 27, 28, 30, 31, 33, 34 and 36 demonstrate high sensitivities to cloud physical structures. These 13 wavebands cover the visible, near-infrared, and thermal infrared bands. Radiances scattered by clouds at visible and near-infrared demonstrate the characteristics of particle size and optical depth. Radiances emitted by clouds at thermal infrared bands are associated with cloud height. The radiances at these 13 wavebands are then used as representatives to analyze their relationships to cloud physical structures, which are reported in the following sections.

## 4. Principle and Methodology of SRaDM

### 4.1 Physical Parameters Defining Cloud Physical Structure

Cloud physical structure is a unified name for the physical properties of a cloud profile. The name is abstract but specific physical parameters are required to define cloud physical structures. According to previous research and what CPR can measure, 14 physical parameters are used to define the physical structure of CPR cloud profiles in this paper (see Table 2). These parameters denote a cloud's microphysical characteristics (i.e. particle phase, particle size) and macrophysical properties (i.e., cloud height, cloud depth, or thickness).

### 4.2 Qualifying Changes of Physical Structure

The units of the 14 physical parameters are not uniform. Differ-

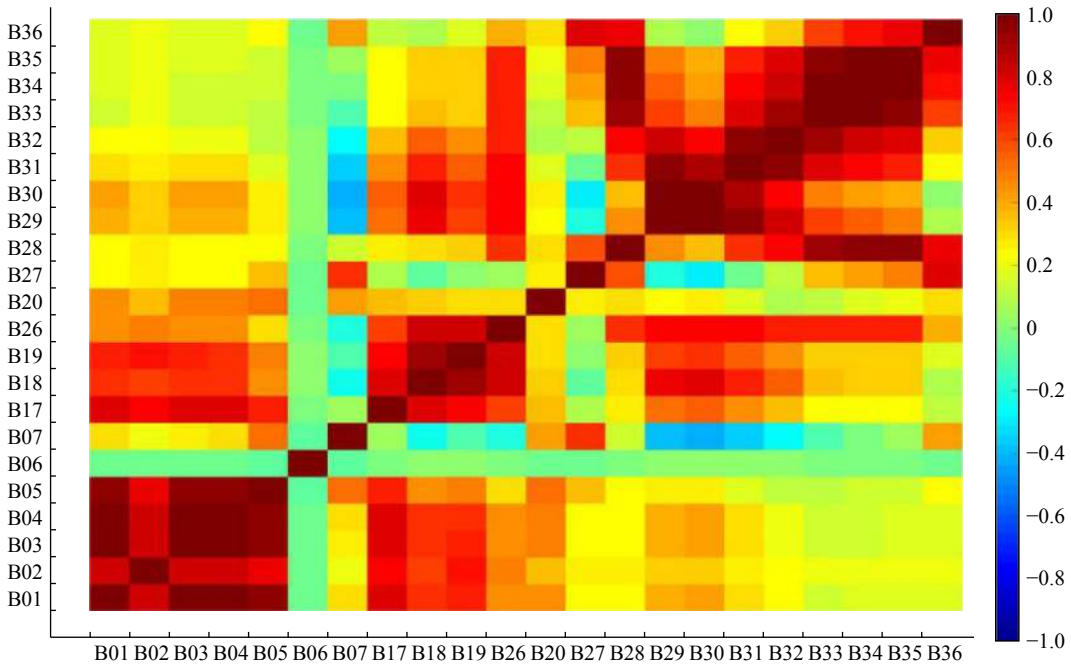


**Figure 3**. Pearson's correlation coefficients between 22 wavebands for the clouds in Figure 2. The $x$-axis and $y$-axis indicate the waveband number of MODIS. The letter "B" means "waveband".

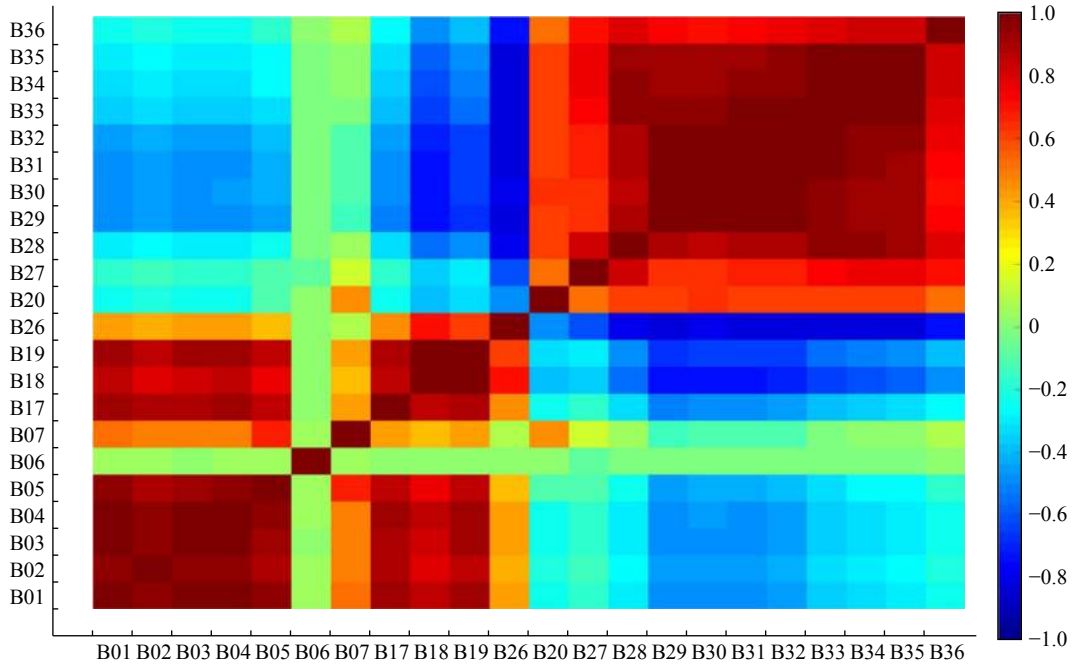


**Figure 4**. Correlation coefficients between 22 spectral bands, which are calculated from all radiances of clouds collected from January 2007 to December 2010. The *x*-axis and *y*-axis are the same as in Figure 3.

**Table 2.** The 14 physical parameters describing cloud physical structure

| | |
|---|---|
| 1 | Maximum top height |
| 2 | Lowest height |
| 3 | Mean height |
| 4 | Standard deviation of height |
| 5 | Maximum $Z_e$ (Max$Z_e$) |
| 6 | Height for Max$Z_e$ |
| 7 | Minimum $Z_e$ (Min$Z_e$) |
| 8 | Height for Min$Z_e$ |
| 9 | Mean $Z_e$ |
| 10 | Standard deviation of $Z_e$ |
| 11 | Maximum temperature |
| 12 | Lowest temperature |
| 13 | Mean temperature |
| 14 | Standard deviation of temperature |

ences (changes) of physical structure between two cloud profiles cannot be obtained directly. Here, the Standardized Euclidean distance—an advanced version of the Euclidean distance—is introduced and used to calculate the difference. It calculates the Euclidean distance after standardizing all attributes of the object. For the calculation of differences in physical structure, the 'object' is the physical structure and the 'attributes' are the 14 physical parameters. One attribute array (termed $P_A$) is standardized as follows:

$$P_A^* = (P_A - m)/s, \tag{2}$$

where $P_A^*$ is the array after standardization, $s$ is the standard deviation of $P_A$, and $m$ is the mean value of $P_A$. Then, the Standardized Euclidean distance between 'objects' $P_A$ ($a_1$, $a_2$, $a_3$, ..., $a_n$) and $P_B$ ($b_1$, $b_2$, $b_3$, ..., $b_n$) is defined as

$$D = \sqrt{\sum_{k=1}^{n}\left(\frac{a_k - b_k}{s_k}\right)^2}, \tag{3}$$

where $s_k$ is the standard deviation of each attribute array, which is calculated based on all cloud profiles; and $n$=14 for 'object'–physical structure, while $n$= 13 for 'object'– spectral radiance. Hereinafter, the Standardized Euclidean distance in physical structure is termed $D_{st}$, which is also expressed as 'physical difference'. The Standardized Euclidean distance in radiances at multiple wavebands is termed $D_{rd}$, which is also expressed as 'radiative difference'. In this paper, the $s_k$ used for the calculation of $D_{rd}$ is set as 6.09, 101.53, 21.47, 1.77, 38.09, 33.03, 7.16, 0.17, 0.38, 0.74, 1.72, 1.54, and 0.60, respectively; and the $s_k$ used for the calculation of $D_{st}$ is set as 3.61, 2.44, 2.59, 13.26, 11.78, 2.76, 4.87, 3.55, 8.93, 3.38, 13.16, 20.60, 13.17, and 6.81, respectively. For two cloud profiles with the same structures, $D_{st}$=0. A large $D_{st}$ means there is a considerable difference in the physical structure. Likewise, a large $D_{rd}$ means a substantial difference in multi-spectral radiances.

### 4.3 Relationship Between $D_{st}$ and $D_{rd}$

$D_{st}$ and $D_{rd}$ quantify the difference in physical structures and in spectral radiances between two cloud profiles. A group of cloud profiles, observed on 15 December 2008, reveals a potential relation between $D_{rd}$ and $D_{st}$ (see Figure 5).

As shown in Figure 5a, the physical structures of clouds change greatly along the flight path. The cloud layer flips between one and two. The cloud thickness fluctuates from 10 to 1 km. The cloud top height ranges from 11.3 to 1.2 km. For convenience and

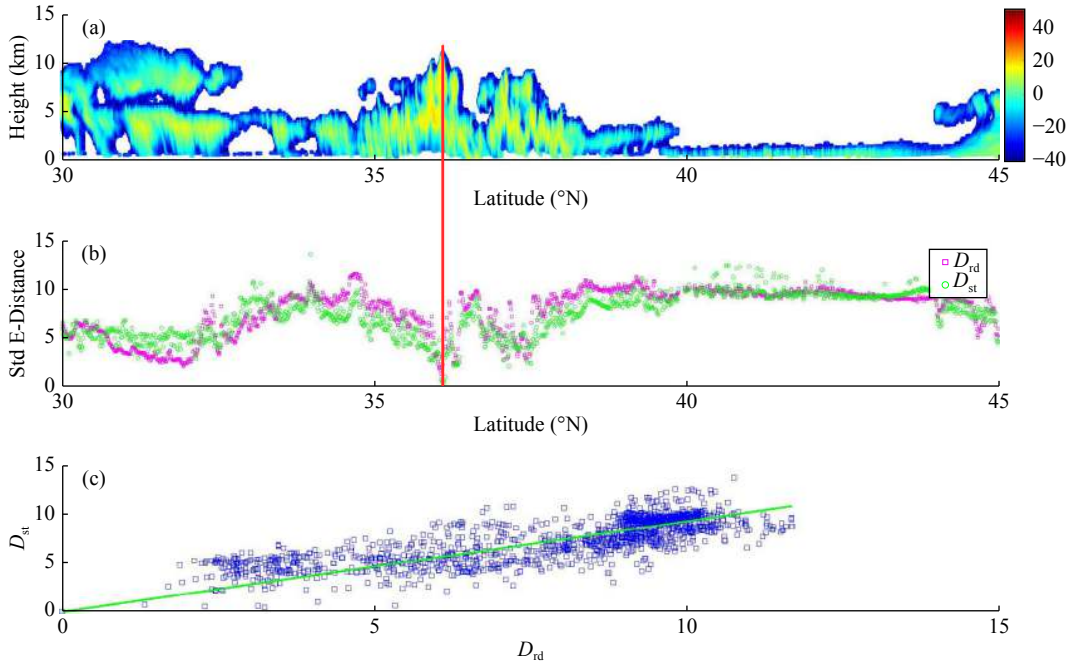


**Figure 5**. (a) Cloud profiles measured by CPR on 15 December 2008; (b) the $D_{st}$ and $D_{rd}$ between the "red" profile and other profiles; (c) relationship between $D_{st}$ and $D_{rd}$: radiative differences increase with an increase in physical difference.

simplicity, a cloud profile sample (at the latitude of 36°N, indicated by the red line in Figure 5a, termed 'Pr') is chosen as a representative to demonstrate the distributions of $D_{rd}$ and $D_{st}$ with other profiles. It should be noted that each cloud profile in Figure 5a can be used as a reference profile in the calculation of $D_{rd}$ and $D_{st}$. The $D_{st}$ and $D_{rd}$ values are shown correspondingly in Figure 5b. Cloud profiles near the Pr profile have similar physical structures. Correspondingly, their $D_{st}$ and $D_{rd}$ values are lower than those of other cloud profiles. Cloud profiles around the latitudinal range of 40°N–42°N show markedly different cloud heights and thicknesses relative to the Pr profile. Correspondingly, $D_{st}$ and $D_{rd}$ increase greatly. Figure 5c presents the relationship between $D_{rd}$ and $D_{st}$. It can be seen that the radiative differences increase with an increase in physical difference.

More cases (see Figure 6) show that the radiative difference will generally increase with an increase in physical difference. It should be noted, however, that the radiative differences also include differences caused by other factors, such as measurement uncertainties, solar position, and atmospheric conditions. Ideally, those differences should be excluded to obtain the 'real' radiative difference between two cloud profiles. To minimize differences caused by the surface, only clouds over an ocean area are studied. The moving speed of the satellite is approximately 420 km/min; it takes around 4 min to fly from the latitude of 30° to 45°. To minimize differences caused by the atmosphere, the observation time interval of cloud profiles is restricted to within 4 min. Currently, it is hard to identify the actual radiative difference because of limited knowledge regarding other factors, such as measurement uncertainties. Nonetheless, the analysis here shows that there is an obvious monotonic relationship between the radiative difference and the physical difference. That is, when the radiative difference is large, the physical difference is large, too. When the radiative difference decreases, so does the physical difference.

## 5. Experimental Application of SRaDM

The analysis above proves that variations of radiative difference are clearly related to the variations of physical difference. It can be concluded that the physical difference is small and fluctuates in a small range if the radiative difference is negligible. Based on this law, cloud profiles of unknown physical structure could be revealed from other profiles of similar spectral radiances and of known physical structure. One CPR footprint covers a breadth of only about 1.4 km across the flight track. Physical structures of cloud profiles near but not on the flight path can be detected through collocation of other cloud profiles with the smallest radiative difference. That is, the physical structure of the collocated cloud profile could be used as a substitute to determine the physical structure of the particular cloud of interest. The method to achieve this, i.e., to reveal cloud physical structure through application and collocation of radiative differences, is what we have been referring to as SRaDM—the smallest-radiance-distance method.

To find optimum collocation profiles for use in the experiments, several items were considered and actions were taken to minimize the influence of other factors:

(1) Since the radiances measured by MODIS are subject to atmospheric influence, clouds under steady weather conditions would be preferable.

(2) CloudSat flies approximately 1.5 min after Aqua, at a speed of about 7 km/s. If the searching radius is set as $r$=200 km, the observation time interval is within 1 min, a time short enough that we can assume minimal change in atmosphere and incident solar radiation.

(3) To screen out improper collocation, the top five collocation profiles of SRaDM are selected as candidates. The profile of the

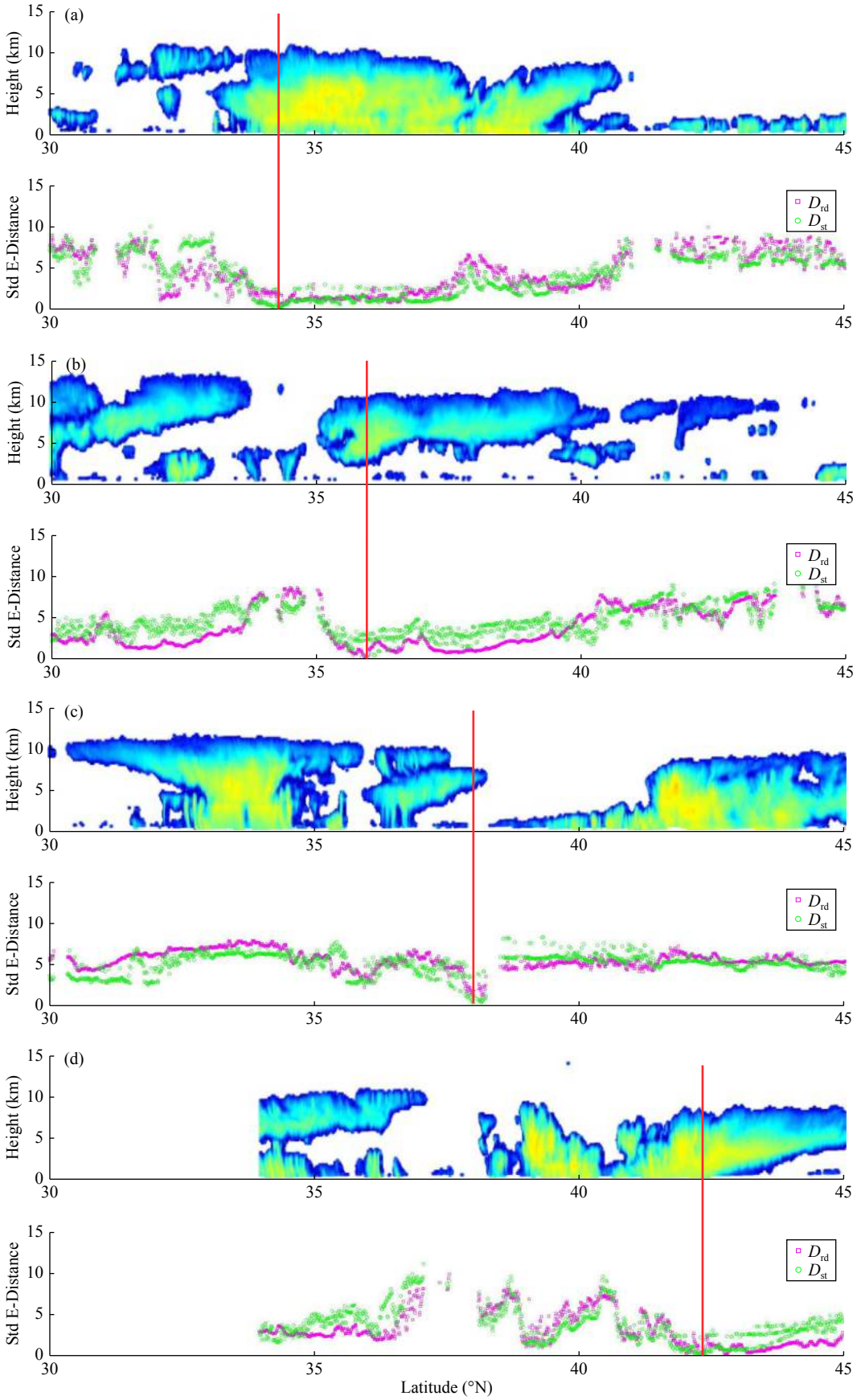


**Figure 6**. Distribution of $D_{rd}$ and $D_{st}$ from other cases: (a) clouds that occurred on 8 January 2007; (b) clouds that occurred on 17 April 2007; (c) clouds that occurred on 30 January 2008; (d) clouds that occurred on 14 February 2008.

closest position among the five profiles is then used as the final collocation profile.

(4) It is hard to suggest a detailed threshold of radiative difference indicating whether two cloud profiles have close physical structures. Statistics show that the smaller the radiative difference, the greater the probability of getting a smaller physical difference. According to analyses of more cases, changes in cloud physical structures are restricted in a short range when the radiative difference is less than three. When radiative differences are less than one, 90% of physical differences are less than 1.5. In our experiments, collocation profiles are initially found using a $D_{rd}$ threshold of one.

An experiment (Figure 7) is designed to demonstrate the performance of SRaDM. Clouds on the CPR path are observed by both MODIS and CPR. Clouds near but not on the CPR path are observed only by MODIS. In this experiment, physical structures of cloud profiles on the CPR path are supposed to be unknown at first and are the objects to be revealed by analysis of radiative data. For each cloud profile of 'unknown' physical structure, the radiative differences to other profiles on the CRP path within 200 km are calculated and compared to find the collocation profile. These successfully described cloud profiles then form a new scanning path that is compared with the observations of CPR. The original physical structures observed by CPR are given in Figure 7a. Along the CPR path, cumulus clouds, stratus clouds, cirrus clouds, and altostratus clouds appear. The physical structures determined from collocation profiles are presented in Figure 7b. Figure 7c shows the radiative differences and physical differences between Figure 7a and Figure 7b. It can be seen that most derived profiles show similar physical structures to the CPR observations. A few cloud profiles fail to achieve collocation profiles because collocation conditions are not satisfied ($D_{st}$>3). On the whole, SRaDM performs well in revealing cloud physical structures.

Using SRaDM, the physical structures of profiles outside of the CPR path can also be derived. An experiment in which SRaDM revealed physical structures within a rectangular area is presented in Figure 8. The clouds in the experiment are from 2 June 2008. The white box in Figure 8a indicates where the physical structures are to be derived. A schematic diagram of the collocation process is shown in Figure 8b. For the pixel at ($x_i$, $y_j$) of unknown physical structure, the radiative differences to other profiles on the CPR path within 200 km are calculated. The collocation pixel at ($x_s$, $y_t$) of the smaller radiative difference and nearest position is identified. The physical structure of a pixel at ($x_s$, $y_t$) is then assigned to the profile at ($x_i$, $y_j$). After all collocation profiles in the square area are achieved, a 3D cloud field is obtained. The liquid effective radius (LER; units: μm) and liquid water content (LWC; units: g/m$^3$) of each grid in the cloud are shown in Figure 8c and Figure 8d. The LER and LWC are provided by the 2B-CWC-RVOD and 2C-ICE products.

Currently, it is difficult to examine the performance of SRaDM in revealing 3D cloud field owing to a shortage of in-situ observations. As a potential alternative, indirect examination via a 3D radiative transfer model could be considered. Radiances simulated by such a model, based on SRaDM-determined cloud fields, could be

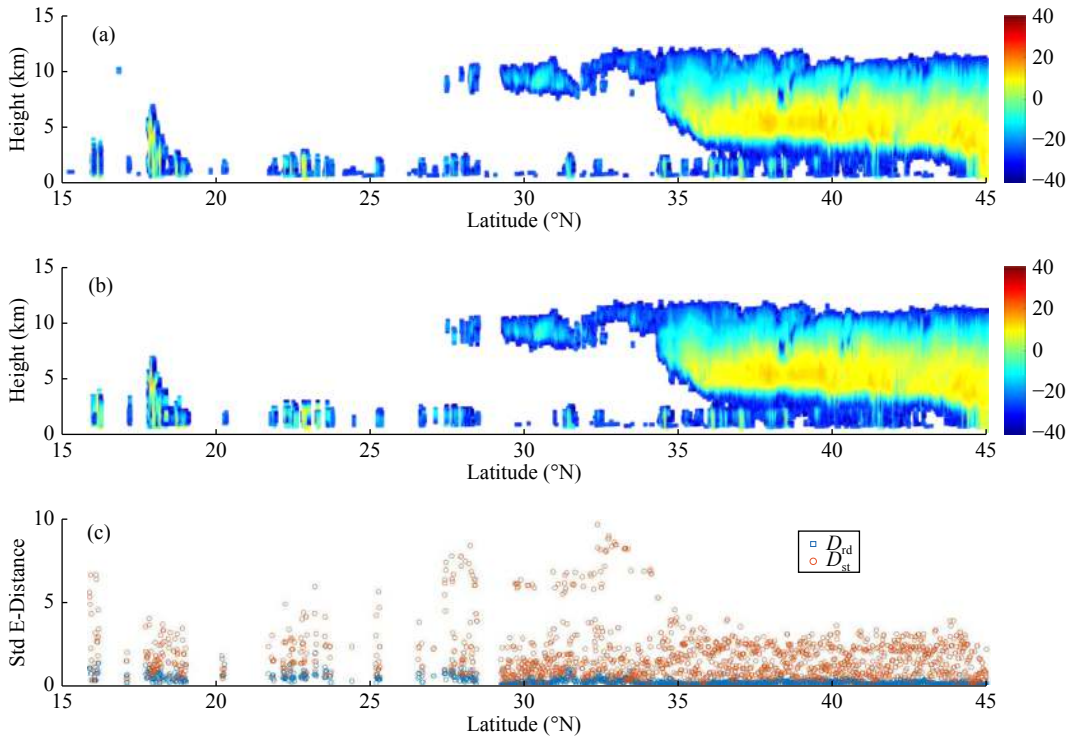


**Figure 7**. Experiment in which physical structures of clouds on the CPR path are revealed: (a) radar reflectivity factors observed by CPR on 24 November 2010; (b) radar reflectivity factors based on SRaDM analysis; (c) the $D_{st}$ and $D_{rd}$ of profiles between the observed and derived radar reflectivity factors.

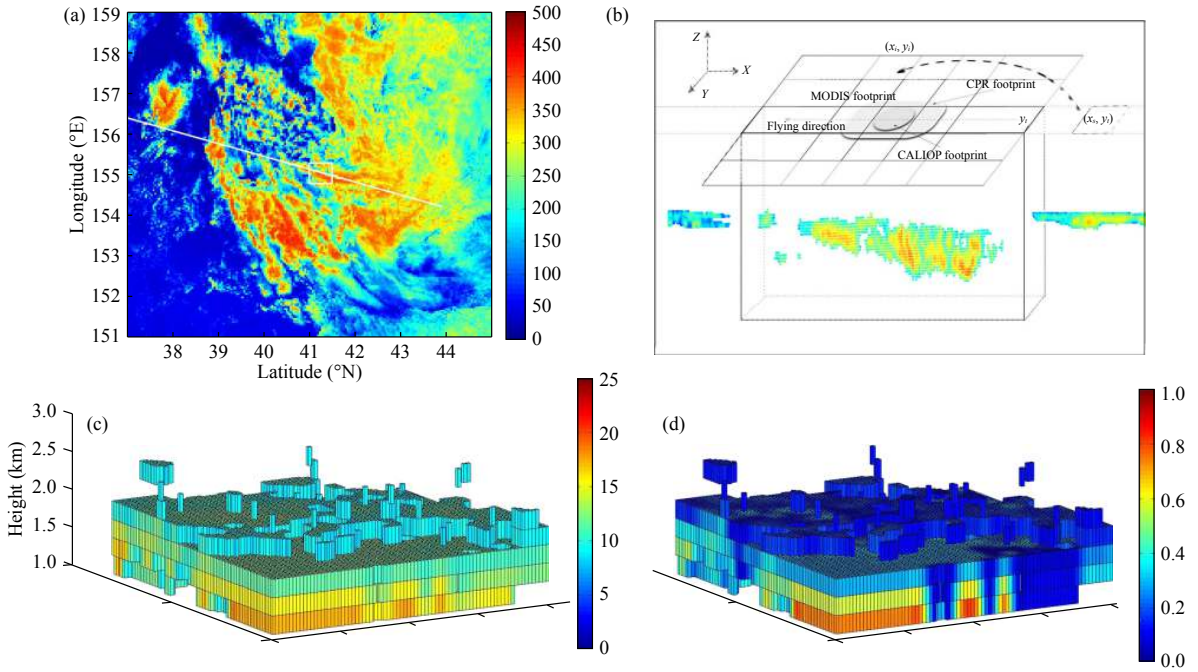


**Figure 8**. SRaDM determination of physical structures for 3D cloud fields: (a) radiance at waveband 1 measured by MODIS on 2 June 2008; (b) schematic diagram of the collocation process; (c) LERs (units: μm) of the 3D cloud fields revealed by SRaDM; (d) LWC (units: g/m$^3$) of the of the 3D cloud fields.

compared to MODIS observations. Then, validation experiments might be achievable via model simulations. However, such simulations will challenge the validation process because errors in the model's calculation and retrieval of physical parameters will cause differences between the simulations and observations. More work on validation will be performed in the future.

## 6. Summary and Discussion

Clouds suspended in the atmosphere are diverse in terms of their structures and physical properties. The formation and evolution of clouds follow certain rules that are affected and restricted by the external environment. Radiative characteristics of clouds reflect their physical properties.

Passive remote sensing measures these radiative characteristics. Radar is a powerful tool for exploring the physical structure of clouds. The measurements of MODIS and CPR onboard the A-train satellite platform offer a chance to study the relationship between radiative characteristics and physical structures of clouds. In this paper, the spectral bands of MODIS are compared through correlation analysis, and radiances at 13 spectral bands are finally used to describe the radiative properties of cloud profiles. According to previous research and what CPR can measure, 14 physical parameters are used to define the physical structure of clouds. The Standardized Euclidean distance is introduced to quantify differences in multi-spectral radiances and in physical structures between cloud profiles. Statistical analysis based on four years of data shows that there is a significant relationship between cloud physical difference and radiative difference. That is, the physical difference between two cloud profiles increases with an increase in radiative difference, especially for profiles of clouds whose physical structures change greatly.

Radar penetrates clouds and measures interior physical structures. However, limitations of their field of view (FOV) is a drawback of the radars onboard satellites, whereas spectroradiometers have a relatively larger FOV. According to the method presented in this paper, i.e., SRaDM, it is possible to understand the physical structures of clouds in relatively broader regions based on multi-spectral radiances. The two experiments carried out show the possibilities and success in determining cloud physical structures from radiative data. It should be noted that the method presented here requires collocation profiles (candidate profiles) with lower radiative differences, so the probability of obtaining an ideal collocation profile will increase if there are many candidate profiles. For a cloud profile with highly complex structure, the complexity of its distribution features will increase the difficulty of finding a collocation profile. Therefore, SRaDM is more suitable for clouds of horizontally uniform distribution.

SRaDM offers a new pathway for deriving physical structures of 3D cloud fields via the use of multi-spectral radiance data. However, paucity of in situ observational data requires that further validation of the method is needed. To address this, model simulations via 3D radiative transfer models will be performed in our future work. Meanwhile, measurements at more spectral bands, such as the microwave bands, may become available as technology advances, and thus it is hoped that the potential of SRaDM to reveal physical structure will increase accordingly with these anticipated measurement advances.

## Acknowledgments

This work is supported by the National Natural Science Foundation of China (Grant 41775032) and Key Research Program of Frontier Sciences, Chinese Academy of Sciences (Grant QYZDY-

SSW-DQC027). We appreciate valuable suggestions and insightful instructions from the reviewers. We also acknowledge the CloudSat team and Aqua team for sharing CPR and MODIS product data that made our research possible.

## References

Ackerman, S. A., Holz, R. E., Frey, R., Eloranta, E. W., Maddux, B. C., and McGill, M. (2008). Cloud detection with MODIS. Part II: validation. *J. Atmos. Oceanic Technol.*, *25*(7), 1073–1086. https://doi.org/10.1175/2007JTECHA1053.1

Alexandrov, M. D., Marshak, A., and Ackerman, A. S. (2010). Cellular statistical models of broken cloud fields. Part I: theory. *J. Atmos. Sci.*, *67*(7), 2125–2151. https://doi.org/10.1175/2010JAS3364.1

Barker, H. W., Jerg, M. P., Wehr, T., Kato, S., Donovan, D., and Hogan, R. J. (2011). A 3D cloud-construction algorithm for the EarthCARE satellite mission. *Quart. J. Roy. Meteor. Soc.*, *137*(657), 1042–1058. https://doi.org/10.1002/qj.824

Baum, B. A., Paul Menzel, W., Frey, R. A., Tobin, D. C., Holz, R. E., and Ackerman, S. A. (2012). MODIS cloud-top property refinements for Collection 6. *J. Appl. Meteor. Climatol.*, *51*(6), 1145–1163. https://doi.org/10.1175/JAMC-D-11-0203.1

Frey, R. A., Ackerman, S. A., Liu, Y. H., Strabala, K. I., Zhang, H., Key, J. R., and Wang, X. G. (2008). Cloud detection with MODIS. Part I: improvements in the MODIS cloud mask for collection 5. *J. Atmos. Oceanic Technol.*, *25*(7), 1057–1072. https://doi.org/10.1175/2008JTECHA1052.1

Görsdorf, U., Lehmann, V., Bauer-Pfundstein, M., Peters, G., Vavriv, D., Vinogradov, V., and Volkov, V. (2015). A 35-GHz polarimetric Doppler radar for long-term observations of cloud parameters-description of system and data processing. *J. Atmos. Oceanic Technol.*, *32*(4), 675–690. https://doi.org/10.1175/JTECH-D-14-00066.1

Heymsfield, A., Winker, D., Avery, M., Vaughan, M., Diskin, G., Deng, M., Mitev, V., and Matthey, R. (2014). Relationships between ice water content and volume extinction coefficient from in situ observations for temperatures from 0° to -86°C: implications for spaceborne lidar retrievals. *J. Appl. Meteor. Climatol.*, *53*(2), 479–505. https://doi.org/10.1175/JAMC-D-13-087.1

Khairoutdinov, M., and Kogan, Y. (2000). A new cloud physics parameterization in a large-eddy simulation model of marine stratocumulus. *Mon. Wea. Rev.*, *128*(1), 229–243. https://doi.org/10.1175/1520-0493(2000)128<0229:ANCPPI>2.0.CO;2

Marchand, R. (2013). Trends in ISCCP, MISR, and MODIS cloud-top-height and optical-depth histograms. *J. Geophys. Res. Atmos.*, *118*(4), 1941–1949. https://doi.org/10.1002/jgrd.50207

Nakajima, T., and King, M. D. (1990). Determination of the optical thickness and effective particle radius of clouds from reflected solar radiation measurements, Part I: theory. *J. Atmos. Sci.*, *47*(15), 1878–1893. https://doi.org/10.1175/1520-0469(1990)047<1878:DOTOTA>2.0.CO;2

Prigarin, S. M., and Marshak, A. (2009). A simple stochastic model for generating broken cloud optical depth and cloud-top height fields. *J. Atmos. Sci.*, *66*(1), 92–104. https://doi.org/10.1175/2008JAS2699.1

Sekelsky, S. M., Ecklund, W. L., Firda, J. M., Gage, K. S., and McIntosh, R. E. (1999). Particle size estimation in ice-phase clouds using multifrequency radar reflectivity measurements at 95, 33, and 2.8 GHz. *J. Appl. Meteor.*, *38*(1), 5–28. https://doi.org/10.1175/1520-0450(1999)038<0005:PSEIIP>2.0.CO;2

Stevens, B., Moeng, C. H., and Sullivan, P. P. (1999). Large-eddy simulations of radiatively driven convection: sensitivities to the representation of small scales. *J. Atmos. Sci.*, *56*(23), 3963–3984. https://doi.org/10.1175/1520-0469(1999)056<3963:LESORD>2.0.CO;2

Winker, D. M., Vaughan, M. A., Omar, A., Hu, Y. X., and Powell, K. A. (2009). Overview of the CALIPSO mission and CALIOP data processing algorithms. *J. Atmos. Oceanic Technol.*, *26*(11), 2310–2323. https://doi.org/10.1175/2009JTECHA1281.1